Chemical Engineering Science 292 (2024) 119987

Contents lists available at ScienceDirect

Chemical Engineering Science

journal homepage: www.elsevier.com/locate/ces

Modelling of the leaching process by the extended quadrature method of moments

Mohsen Shiea *, Luigi Crema, Edoardo Gino Macchi

Center for Sustainable Energy, Fondazione Bruno Kessler, Via Sommarive 18, 38123 Trento, Italy

ARTICLE INFO

Keywords:
Leaching
Modelling
Population balance equation (PBE)
Extended quadrature method of moments (EQMOM)
Shrinking-core model

ABSTRACT

An approach based on the extended quadrature method of moments (EQMOM) has been developed to solve the population balance equation written for the evolution of shrinking-core particles in transient leaching processes. It has been shown that the EQMOM can naturally address the dependency of the shrinkage-core model on the unreacted core size and outer size of particles. The approach has been validated by comparing its predictions with either analytical or reference solutions for several test cases. Moreover, the approach has been employed to simulate an experimental leaching process taken from the literature. The obtained results confirm the significance of considering the particle size distribution in the simulation of the leaching process, hence the importance of solution methods such as that presented in this work. Finally, it has been shown that the proposed approach is also useful for the simulation of the dissolution process with shrinking particles.

1. Introduction

A comprehensive description of the leaching process requires a modelling tool capable to follow the evolution of particles when the particle size distribution (PSD) is not narrow enough to adopt mono-sized modelling approaches [1,2]. In this context, a systematic approach for taking into account the PSD is population balance modelling (PBM) [1,3–6], which essentially writes a population balance equation (PBE) in terms of the PSD. While the application of PBM to the leaching process is well established, the solution methods applied to the PBE for this process still have some limitations. LeBlanc and Fogler [1] used the method of characteristics to solve a PBE for describing the dissolution of solid particles under mass-transfer and surface-reaction controlling regimes. Accordingly, the initial particle size distribution can have the form of either a log-normal or Rosin-Rammler (known also as Weibull) distribution. However, they assumed an excess solvent concentration that essentially remains constant over the entire process, which is not always the case. Hänchen et al. adopted the same approach to describe the dissolution of olivine particles with bi-modal initial distributions [7]. They assumed that the dissolution rate depends on neither the solution concentration nor the particle size. It is noteworthy that the above-mentioned approaches can be adopted to simulate the leaching process only if the process is controlled by the surface-reaction, i.e., the diffusion in the inert-layer and liquid film around particles is negligible. Crundwell and Bryson [8] simulated a steady-state continuous zinc pressure leaching reactor by coupling the PBE with the mass and energy balances for the reactant concentration and reactor temperature, respectively. They derived a steady-state PBE for the number density of particles in terms of the particle size. Moreover, they assumed a general shrinking-core kinetic model, and therefore, their method can be applied to cases other than surface-reaction rate limited cases. In their approach, the steady-state PBE is first integrated by the method of integrating factors and then is solved numerically by using the trapezoidal integration with Richardson extrapolation. It is evident that the numerical integration requires the discretization of the size space, which is not a straightforward task, particularly when the size distribution is broad, or it has steep changes, or its shape changes significantly. Moreover, the solution method is not suitable for transient systems, e.g., batch reactors. Another numerical method for the solution of the PBE in leaching applications is the method of lines [5,9], which can be applied to transient cases. Likewise, this method needs the discretization of the size space with the same shortcomings mentioned earlier. Gbor and Jia [2] proposed a method to consider the PSD in the calculation of the conversion for the leaching process, which essentially makes use of a function that defines the unreacted fraction of particles of a given size. However, they assumed a constant reactant concentration in the calculation of the conversion. Moreover, their method requires the division of the PSD into discrete sizes when the diffusion in the inert-layer around par-

* Corresponding author.
E-mail address: mshiea@fbk.eu (M. Shiea).

https://doi.org/10.1016/j.ces.2024.119987
Received 30 October 2023; Received in revised form 29 February 2024; Accepted 6 March 2024
Available online 12 March 2024

ticles is not negligible. Another common method for the solution of the PBE is the method of classes or sectional method [10]. Zhao et al. adopted this method to simulate the reactive dissolution of particle agglomerates that undergo the breakage simultaneously [11]. In another work, Dale et al. used the sectional method to describe the aggregation and dissolution of nanoparticles [12]. However, the main disadvantage of this method is that a relatively large number of classes is required to achieve a satisfactory accuracy [13]. Moreover, to the best of our knowledge, no published work has adopted the method of classes with the shrinking-core kinetic model.

It is noteworthy that closed-form solutions for the leaching process are present in the existing literature, however, they lack generality. For instance, Giona et al. derived a closed-form solution for the PBE by assuming a large excess of the reactant [6]. In addition to the excess reactant assumption, their method requires the discretization of the size space if the dissolution kinetics is controlled by both the surface reaction and mass-transfer in the boundary layer around particles.

In the present work, we propose a general approach to solve the PBE in transient leaching processes, which overcomes the previously mentioned shortcomings. In fact, it can be adopted to simulate the leaching process in spatially homogeneous batch reactors without making any assumption about the controlling regime or reactant concentration. The proposed approach is based on the extended quadrature method of moments (EQMOM) introduced by Yuan et al. [14], which is adapted to the shrinking-core model. This adaption is indeed a novelty of this work as it allows to consider both the (constant) distribution of the particle outer size and the (varying) distribution of the particle core size in evaluation of the shrinking-core model. After elaborating the approach, its advantages are verified by assessing its performance in several test cases, including a real experimental leaching problem. Additionally, it is shown that the proposed method is applicable to dissolution applications, i.e., cases with shrinking particles.

2. Population balance modelling of the leaching process

The central concept of PBM is the particle distribution function, $n(\boldsymbol{\xi};\mathbf{x},t)$, known also as the number density function (NDF), which represents the distribution of a given population of particles over some properties of interest $\boldsymbol{\xi}$ in a specific spatial position $\mathbf{x}$ and time t. By definition, $n d\boldsymbol{\xi} d\mathbf{x}$ is the number of particles with properties between $\boldsymbol{\xi}$ and $\boldsymbol{\xi} + d\boldsymbol{\xi}$ that are located at spatial position between $\mathbf{x}$ and $\mathbf{x} + d\mathbf{x}$. Some examples of particle properties $\boldsymbol{\xi}$ are size, velocity, concentration and temperature that in fact determine the particle state. In the population balance literature, these properties are called internal coordinates, whereas the spatial position of particles, $\mathbf{x}$, is called the external coordinate. Moreover, the internal and external coordinates together form the particle phase space through which particles are transported with certain velocities or rates. In 3-dimensional problems with N_ξ internal coordinates, the phase space has $N_\xi + 3$ dimensions. This allows us to restate the definition of $n(\boldsymbol{\xi};\mathbf{x},t)$ as the number of particles per unit phase space. Now, the evolution of particles in the phase space can be described through a balance equation written in terms of $n(\boldsymbol{\xi};\mathbf{x},t)$, known as the PBE [15],

$$\frac{\partial n}{\partial t} + \nabla_{\mathbf{x}} \cdot (\mathbf{U}n) + \nabla_{\boldsymbol{\xi}} \cdot (\dot{\boldsymbol{\xi}} n) = B - D\,, \tag{1}$$

where, the second and third terms on the left-hand side of Eq. (1) represent the transport of particles in the physical space by the particle velocity $\mathbf{U}$ and in the state space by the rate $\dot{\boldsymbol{\xi}}$, respectively. B and D are the source terms that describe respectively the birth and death of particles due to discontinuous processes such as the aggregation and breakage of particles. The choice of internal coordinates and discontinuous processes in Eq. (1) is problem-dependent, and therefore, we introduce the leaching process before adapting the PBE for it.

In the leaching process, solid particles are brought into contact with a solution containing a leaching agent A (usually an acid), which dissolve a target compound B in the solid phase. The reaction can be written as

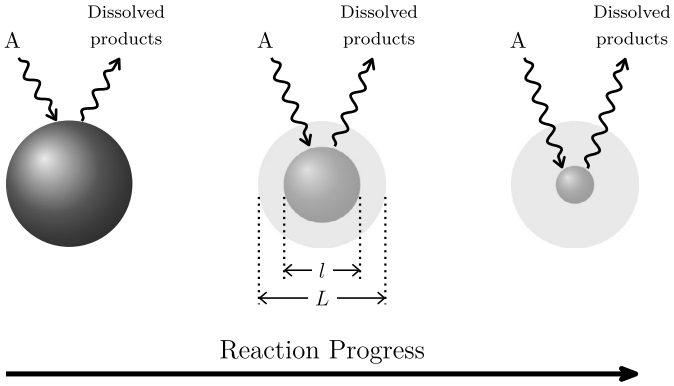

Fig. 1. Shrinking-core model. The leaching agent A diffuses from the bulk solution to the particle surface, where the reaction occurs between A and the active material in the particle. As the reaction proceeds, an inert layer remains around the particle, and therefore, A needs to diffuse through this layer to reach the surface of the unreacted core of the particle, where the reaction can take place. l and L are the core and outer size of the particle, respectively.

$$\mathrm{A}_{(\mathrm{l})} + b\,\mathrm{B}_{(\mathrm{s})} \longrightarrow \text{dissolved products}, \tag{2}$$

where, the stoichiometric ratio b defines the number of moles of B dissolved by one mole of A. A widely adopted approach for the description of the leaching process is the shrinking-core model that assumes the formation of an inert layer of a solid product around particles due to the reaction. Therefore, each solid particle is considered as an unreacted core rich in B surrounded by an inert layer. At the beginning of the process, solid particles are fully unreacted. As the reaction proceeds, the unreacted core shrinks and the thickness of the inert layer increases. Therefore, in general, the process can be viewed as three steps: 1) the diffusion of A in the liquid film around particles, i.e., from the bulk solution to the particle surface, 2) the diffusion of A in the inert layer, 3) the reaction between A and B at the surface of the unreacted core. The shrinking-core model, illustrated in Fig. 1, can be expressed mathematically by the following kinetic formula, as detailed by Levenspiel [16],

$$G(l,t) \equiv \frac{\mathrm{d}l}{\mathrm{d}t} = \frac{-2bC_{\mathrm{A}}}{\rho_{\mathrm{B}}\left[\frac{1}{k_{\mathrm{s}}} + \frac{1}{2\mathscr{D}_{\mathrm{e}}}(l - l^2/L) + \frac{1}{k_{\mathrm{f}}}(l/L)^2\right]}\,. \tag{3}$$

Essentially, Eq. (3) expresses the rate of change in particle (core) size as a thermodynamic driving force divided by the total resistance due to the surface reaction, diffusion of A in the inert layer, and mass transfer in the liquid film around particles. Here, l and L denote the core and outer size of the particle in meters, respectively (see Fig. 1). C_{A} is the molar concentration of A in the bulk solution and ρ_{B} the molar concentration of B in the solid particle. k_{s}, $\mathscr{D}_{\mathrm{e}}$ and k_{f} are the surface reaction rate ($\mathrm{m\,s^{-1}}$), effective diffusion coefficient of A in the inert layer ($\mathrm{m^2/s}$), and the mass transfer coefficient in the liquid film around the particle ($\mathrm{m\,s^{-1}}$), respectively. In the shrinking-core model, the main property of particles is the core size, l. Moreover, the outer size of particles, L, is assumed constant, i.e., the outer layer is not dissolved. It is noteworthy that Eq. (3) can also be applied to dissolution problems, i.e., when no inert layer forms, by setting $l \equiv L$, which cancels the contribution of the inert layer to the total resistance. In this case, l refers simply to the particle size.

Returning to the PBE, we take l as the only internal coordinate following the shrinking-core model. Moreover, the aggregation and breakage of particles is neglected since it is a common practice in the modelling of leaching processes. By using these assumptions and directing our attention to a spatially homogeneous batch reactor, Eq. (1) can be simplified as

Table 1
List of non-dimensional variables, their corresponding dimensional variables, and their definitions.

Non-dimensional variable	Dimensional variable	Definition
l^*	l (m)	$l^* = l/\bar{L}$
t^*	t (s)	$t^* = t/\tau$
G^*	G (m/s)	$G^* = G\tau/\bar{L}$
G'^*	G' (1/s)	Eq. (15)
C_A^*	C_A (mol/m^3)	$C_A^* = C_A/C_A^0$
S^*	S (mol/m^3/s)	$S^* = \tau S/C_A^0$
ρ_B^*	ρ_B (mol/m^3)	$\rho_B^* = \rho_B/C_A^0$

Table 2
List of variables in the transformed size domain, their corresponding variables in non-transformed size domain and their definitions.

Pair of variables		Definition
Transformed domain	Original domain	
l' (-)	l (m)	Eq. (7)
$\hat{f}'$ (-)	$\hat{f}$ (1/m)	$\hat{f}' = \hat{f}\,\mathrm{d}l/\mathrm{d}l'$
G' (1/s)	G (m/s)	Eq. (13)

$$\frac{\partial n}{\partial t} + \frac{\partial (Gn)}{\partial l} = 0\,, \tag{4}$$

where, $n \equiv n(l;t)$ in units of $1/\mathrm{m}^4$. The units of n follow from the fact that the phase space is formed by three spatial coordinates and the particle (core) size with the dimension of length. It is important to remind the reader that G depends in general on both l and L, where the former has a varying distribution governed by Eq. (4) and the latter has a distribution that is constant in time. It will be explained later how the constant distribution of L is considered in evaluation of G.

Moreover, as indicated by Eq. (3), G can depend not only on l but also implicitly on t because C_A can change in time as the reaction proceeds. Therefore, in general, Eq. (1) should be coupled with a balance equation for the concentration of A in the solution, which can be written as

$$\frac{\mathrm{d}C_A}{\mathrm{d}t} = S\,. \tag{5}$$

The source term on the right-hand side of Eq. (5), S, is the consumption rate of A due to the leaching reaction. It can be related to the change in the total concentration of $B_{(s)}$, which in turn, can be calculated through the change in the total volume of particle cores

$$S = \frac{\rho_B}{b}\frac{\mathrm{d}V_c}{\mathrm{d}t} = k_v \frac{\rho_B}{b}\frac{\mathrm{d}}{\mathrm{d}t}\int_0^\infty l^3 n \mathrm{d}l\,, \tag{6}$$

with V_c being the total volume of particle cores. k_v denotes the shape factor, which is equal to $\frac{\pi}{6}$ on the assumption of spherical particles.

2.1. Dimensionless equations

Before introducing the solution method, we make the equations dimensionless. On one hand, it facilitates the numerical solution of the equations. On the other hand, we will use a version of the EQMOM that requires the transformation of the internal coordinate such that any arbitrary bounded interval gets projected onto the interval $[0, 1]$. To enhance understanding of the following derivations, Table 1 lists the non-dimensional variables and their corresponding dimensional variables. In addition, Table 2 shows the pairs of key variables in the transformed-size and original size domain.

Considering the size as the internal coordinate, its transformation is written as

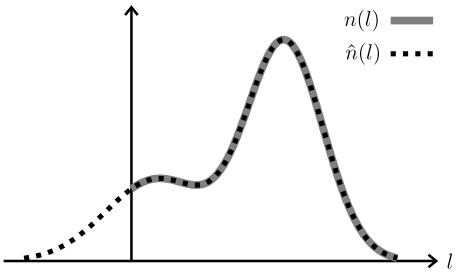

Fig. 2. The pseudo-NDF $\hat{n}(l)$ (black dotted curve) versus NDF $n(l)$ (grey solid curve). The pseudo-NDF extends to the negative domain for numerical reasons without having any physical effect on the modelling of the leaching process.

$$l' = \frac{l - l_{\min}(t)}{l_{\max}(t) - l_{\min}(t)}, \tag{7}$$

where, l' denotes the transformed size, which is also non-dimensional. $l_{\min}(t)$ and $l_{\max}(t)$ are the minimum and maximum bounds of the size, respectively. These bounds change over the time by

$$\frac{\mathrm{d}l_{\min}}{\mathrm{d}t} = G(l_{\min}, t) \quad , \quad \frac{\mathrm{d}l_{\max}}{\mathrm{d}t} = G(l_{\max}, t). \tag{8}$$

For numerical reasons that will be made apparent in the subsequent section, we allow the minimum bound to become non-physically negative. In other words, we allow the existence of particles with negative core sizes that, of course, do not contribute to the consumption of the leaching agent. In the rest of this paper, we call particles with negative core size as "ghost" particles. Thus, we define a pseudo-NDF $\hat{n}$ such that it overlaps the NDF n on the positive size domain but also includes ghost particles. Fig. 2 illustrates an example of the pseudo-NDF in comparison to the NDF. It is noteworthy that at time $t = 0$, we have $\hat{n} = n$. Moreover, in the case of $\hat{n}$, the total number of particles remains constant in contrast to the case of n, where the total number of particles decreases as more and more particle cores are depleted completely by the leaching reaction. The inclusion of negative sizes in the calculations requires us to modify G such that its sign cannot become positive. In this work, we suggest to employ a decaying surface-reaction resistance with the same parameters used in the case of positive sizes, thus

$$G(l,t) = \begin{cases} \dfrac{-2bC_A}{\rho_B\left[\dfrac{1}{k_s} + \dfrac{1}{2\mathscr{D}_e}(l - l^2/L) + \dfrac{1}{k_f}(l/L)^2\right]}, & l > 0 \\ \dfrac{-2bC_A k_s}{\rho_B}\exp(c_d l^*), & l \le 0 \end{cases} \tag{9}$$

where, c_d is an adjustable coefficient and $l^* = l/\bar{L}$. Here, $\bar{L}$ is the length scale, which is defined as the initial average particle size. The above modification guarantees that once the unreacted core of a particle disappears, it cannot be (unphysically) brought into existence. Moreover, the exponential function is included as a decaying factor to prevent excessive decrease of $l_{\min}$. In other words, it controls the broadness of the pseudo-NDF in the negative domain, which can be helpful in cases with negligible surface-reaction resistance, as discussed in the next section. It should be noted that the modified expression for G remains continuous at $l = 0$.

Eq. (8) can be expressed in dimensionless form as

$$\frac{\mathrm{d}l^*_{\min}}{\mathrm{d}t^*} = G^*(l_{\min}, t) \quad , \quad \frac{\mathrm{d}l^*_{\max}}{\mathrm{d}t^*} = G^*(l_{\max}, t), \tag{10}$$

with $t^* = t/\tau$ and $G^* = G\tau/\bar{L}$. Here, τ denotes the time scale, which is defined as the time required to completely leach a particle of size $\bar{L}$ with C_A being constant and equal to the initial concentration of A (C_A^0), hence

$$\tau = \frac{\rho_B}{2bC_A^0}\left[\frac{\bar{L}}{k_s} + \frac{\bar{L}^2}{12\mathscr{D}_e} + \frac{\bar{L}}{3k_f}\right]. \tag{11}$$

For writing the dimensionless PBE, we first define a pseudo-PSD as $\hat{f}(l;t) = \hat{n}(l;t)/\hat{m}_0$, with $\hat{m}_0 = m_0|_{t=0}$. Here, $m_0|_{t=0}$ is the initial number density of particles ($1/m^3$). In fact, it is the first moment of the initial NFD as defined later in Eq. (17). As mentioned previously, $\hat{m}_0$ (in contrast to m_0) does not change in time because by definition, the pseudo-NDF also includes the (ghost) particles with a depleted core. In other words, $\hat{m}_0$ is conserved whereas m_0 is not. Next, we define a non-dimensional distribution $\hat{f}'(l';t)$ in terms of the transformed size l', which is related to $\hat{f}$ by $\hat{f}'\mathrm{d}l' = \hat{f}\mathrm{d}l$. It is important to keep in mind that l' is always between 0 and 1, as defined in Eq. (7), irrespective of the sign of l. In other word, $\hat{f}'(l')$ is always a density function defined on the bounded interval $[0,1]$. Then, we write the following balance equation for $\hat{f}'$

$$\frac{\partial \hat{f}'}{\partial t} + \frac{\partial (G'\hat{f}')}{\partial l'} = 0, \tag{12}$$

where,

$$\begin{aligned} G' \equiv \frac{\mathrm{d}l'}{\mathrm{d}t} &= \left(\frac{\partial l'}{\partial l}\right)_t \frac{\mathrm{d}l}{\mathrm{d}t} + \left(\frac{\partial l'}{\partial t}\right)_l \\ &= \frac{1}{l_{\max} - l_{\min}} \left[G - l' \left(\frac{\mathrm{d}l_{\max}}{\mathrm{d}t} - \frac{\mathrm{d}l_{\min}}{\mathrm{d}t} \right) - \frac{\mathrm{d}l_{\min}}{\mathrm{d}t} \right]. \end{aligned} \tag{13}$$

Since G is continuous in l, then G' is also continuous in l'.

Finally, multiplying Eq. (12) by the timescale (τ) yields the following dimensionless PBE

$$\frac{\partial \hat{f}'}{\partial t^*} + \frac{\partial (G'^* \hat{f}')}{\partial l'} = 0, \tag{14}$$

with,

$$G'^* = \tau G' = \frac{1}{l^*_{\max} - l^*_{\min}} \left[G^* - l' \left(\frac{\mathrm{d}l^*_{\max}}{\mathrm{d}t^*} - \frac{\mathrm{d}l^*_{\min}}{\mathrm{d}t^*} \right) - \frac{\mathrm{d}l^*_{\min}}{\mathrm{d}t^*} \right]. \tag{15}$$

Starting from Eq. (5), the dimensionless balance equation for the concentration of A becomes

$$\frac{\mathrm{d}C^*_{\mathrm{A}}}{\mathrm{d}t^*} = S^*, \tag{16}$$

where, $C^*_{\mathrm{A}} = C_{\mathrm{A}}/C^0_{\mathrm{A}}$ and $S^* = \tau S/C^0_{\mathrm{A}}$.

3. Solution approach for population balance equation

As introduced earlier, we adopt the EQMOM for the solution of Eq. (4), which was developed by Yuan et al. [14]. This method belongs to a family of solution methods known as quadrature-based moment methods (QBMM), which essentially solve for the (low-order) moments of the NDF, m_k, instead of solving the PBE directly. In this work, the moments of the NDF are defined by

$$m_k(t) = \int_0^\infty l^k n(l;t)\mathrm{d}l, \tag{17}$$

with k being the moment order. It is noteworthy that the importance of the low-order moments lies in the fact that they are linked with some measurable quantities of the particle population. For instance, by definition, m_0 is the number density of particles, $k_v m_3$ the particle volume fraction, and m_3/m_2 the Sauter mean diameter.

Considering the dimensionless form of equations derived in the previous section, we continue the discussion by defining the moments of $\hat{f}'$

$$\hat{m}'_k(t) = \int_0^1 l'^k \hat{f}'(l';t)\mathrm{d}l', \tag{18}$$

where, the lower limit of the integration is $l' = 0$ corresponding to $l = l_{\min}$. As mentioned in the previous section, $l_{\min}$ is allowed to take negative values for numerical reasons. This means that the integration in Eq. (18) considers all particles including ghost ones, i.e., those with already depleted cores, whereas the lower limit in Eq. (17) is $l = 0$.

Applying the above moment transformation to the PBE defined in Eq. (14) leads to an integro-differential equation for the moment of order k as follows

$$\frac{\mathrm{d}\hat{m}'_k}{\mathrm{d}t^*} + l'^k G'^*(l')\hat{f}'(l')\Big|_0^1 - \int_0^1 k l'^{(k-1)} G'^*(l')\hat{f}'(l')\mathrm{d}l' = 0. \tag{19}$$

Now we can exploit the advantage of allowing negative sizes and working with the transformed size l' defined in Eq. (7). According to Eq. (15), G'^* is zero at both ends of the interval $[0,1]$, i.e., $l' = 0$ and $l' = 1$ corresponding to $l = l_{\min}$ and $l = l_{\max}$, respectively. As a result, the second term on the left-hand side of Eq. (19) is zero. In fact, if we were to treat the moments of the NDF defined by Eq. (17), this term would not be cancelled in the corresponding equation of the zero-order moment [17,18], and it would be required to know the value of the NDF at size zero. Of course, this is not an issue in the EQMOM method, as it was developed by Yuan et al. [14] to make a continuous approximation of the NDF such that its values at the origin could be calculated. In fact, the simplification of Eq. (19) is not the main reason for using the transformed variable l' (which is devised to let l take negative values) in our formulation of the EQMOM, but we will show that a better reconstruction of the NDF can be obtained by this formulation.

In general, Eq. (19) written for a set of moments presents a closure problem because it involves the (unknown) distribution $\hat{f}'$. The QBMMs cope with this closure problem by approximating the distribution with a quadrature [19]. In the case of the EQMOM, the quadrature is defined as a summation of some weighted kernel density functions (δ_σ). Here, we write the quadrature for $\hat{f}'$

$$\hat{f}'(l') = \sum_{i=1}^{N_{\mathrm{q}}} w'_i \delta_\sigma(l';l'_i), \tag{20}$$

where, w'_i and l'_i are the weight and abscissa of each kernel, respectively. N_{q} is the number of kernels used for the approximation. Here, the kernels are of the same family, with a common parameter σ. The choice of the kernel type is problem-dependent. Moreover, they should satisfy several conditions for being appropriate to the EQMOM [14]. Among different kernels reported in the relevant literature [14,20,21], we restrict our attention to the beta distribution because it is suitable for variables bounded to a finite interval, such as the particle core size in the leaching process. In fact, real particle samples have usually some minimum and maximum initial sizes. In addition, in applications such as the leaching and dissolution (ignoring also the particle aggregation), the particle (core) size decreases in time. And therefore, in such applications, it is legitimate to represent the PSD by a distribution with a bounded support. In this work, the beta kernels are

$$\delta_\sigma(l';l'_i) = \frac{l'^{\lambda_i - 1}(1-l')^{\mu_i - 1}}{\mathcal{B}(\lambda_i,\mu_i)}, \tag{21}$$

with $\lambda_i = l'_i/\sigma$ and $\mu_i = (1-l'_i)/\sigma$, which is equivalent to set the mean of the distribution equal to the kernel abscissa (l'_i). In Eq. (21), $\mathcal{B}(\lambda_i,\mu_i)$ is the beta function. It should be noted that the beta distribution is defined for $l \in [0,1]$, which explains the reason behind the choice of coordinate transformation in Eq. (7).

In the core of the EQMOM, there is an inversion algorithm that calculates the parameters of the quadrature in Eq. (20), i.e., σ, w'_i and l'_i, from a set of $2N_{\mathrm{q}} + 1$ solved moments, which addresses the closure problem of moment equations. Thus, once N_{q} is set, Eq. (19) should be written for the moments of order 0 to $2N_{\mathrm{q}}$. It should be emphasized that in this work, the EQMOM inversion algorithm is applied to the moments of $\hat{f}'$ that is defined on the positive bounded domain $[0,1]$.

We adopt the EQMOM inversion algorithm developed by Nguyen et al. [22]. It is a more robust and efficient version of the original EQMOM

inversion algorithm developed by Yuan et al. [14]. Moreover, it can cope with the realizability issue of moments that will be discussed later.

Let us now continue with the solution of the moment equations by inserting Eq. (20) into Eq. (19), which yields

$$\frac{\mathrm{d}\hat{m}'_k}{\mathrm{d}t^*} - \sum_{i=1}^{N_\mathrm{q}} w'_i \int_0^1 k l'^{(k-1)} G'^*(l')\delta_\sigma(l';l'_i)\mathrm{d}l' = 0. \tag{22}$$

Considering the beta kernel, the integral in Eq. (22) can be estimated by using Gauss-Jacobi integration formula [23] on the interval $[-1,1]$, thus

$$\begin{aligned}
&\int_0^1 k l'^{(k-1)} G'^*(l')\delta_\sigma(l';l'_i)\mathrm{d}l' \\
&= \frac{k}{\mathcal{B}(\lambda_i,\mu_i)} \int_0^1 l'^{(k-1)} G'^*(l') l'^{\lambda_i-1}(1-l')^{\mu_i-1}\mathrm{d}l' \\
&= \frac{k}{2^{(\alpha_i+\beta_i)}\mathcal{B}(\lambda_i,\mu_i)} \int_{-1}^1 \left(\frac{x'+1}{2}\right)^{(k-1)} G'^*\left(\frac{x'+1}{2}\right)(1-x')^{\alpha_i}(1+x')^{\beta_i}\mathrm{d}x' \\
&\approx \frac{k}{2^{(\alpha_i+\beta_i)}\mathcal{B}(\lambda_i,\mu_i)} \sum_{j=1}^{N_i} w'_{i,j} \left(\frac{x'_{i,j}+1}{2}\right)^{(k-1)} G'^*\left(\frac{x'_{i,j}+1}{2}\right),
\end{aligned} \tag{23}$$

where the integral bounds are modified from $[0,1]$ to $[-1,1]$ by a change of variable, $l' = \frac{x'+1}{2}$. In Eq. (23), $\alpha_i = \mu_i - 1$ and $\beta_i = \lambda_i - 1$. Moreover, $x'_{i,j}$ and $w'_{i,j}$ denote the abscissas and weights of the Gauss-Jacobi quadrature, respectively. The reader can find an algorithm to calculate them elsewhere [23]. These abscissas and weights integrate exactly a polynomial of order $2N_i - 1$ multiplied by $(1-x')^{\alpha_i}(1+x')^{\beta_i}$ over the interval of $[-1,1]$. Therefore, if G'^* is a polynomial of order $2N_\mathrm{G}$ or less, then the Gaussian quadrature rule in Eq. (23) is exact for $N_i \geq N_\mathrm{q} + N_\mathrm{G}$. Otherwise, N_i can be chosen large enough (independently from the value of N_q) to make the error of the quadrature rule negligible in comparison to the error due to the first quadrature for $\hat{f}'$, i.e., Eq. (20), [14].

Now, the moment equations can be written as follows

$$\frac{\mathrm{d}\hat{m}'_k}{\mathrm{d}t^*} - \sum_{i=1}^{N_\mathrm{q}} \sum_{j=1}^{N_i} k\varsigma'_{i,j} l'^{(k-1)}_{i,j} G'^*(l'_{i,j}) = 0, \tag{24}$$

with

$$\varsigma'_{i,j} = \frac{1}{2^{(\alpha_i+\beta_i)}\mathcal{B}(\lambda_i,\mu_i)} w'_i w'_{i,j}, \qquad l'_{i,j} = \frac{x'_{i,j}+1}{2}. \tag{25}$$

As noted by Yuan et al. [14], a useful observation is that the second term on the left-hand side of Eq. (24) can be equivalently obtained by approximating $\hat{f}'$ with the point representation

$$\hat{f}'(l') = \sum_{i=1}^{N_\mathrm{q}} \sum_{j=1}^{N_i} \varsigma'_{i,j}\delta(l';l'_{i,j}), \tag{26}$$

instead of Eq. (20). Here, $\delta(l';l'_{i,j})$ are Dirac delta functions centred on the abscissas $l'_{i,j}$. It is important to keep in mind that the weights and abscissas in Eq. (26) are related to both quadratures introduced earlier, i.e., Eq. (20) and Eq. (23). By using the above point representation, the dimensionless PBE, Eq. (14), can be solved by the method of characteristics [14] as follows

$$\frac{\mathrm{d}\varsigma'_{i,j}}{\mathrm{d}t^*} = 0 \quad \text{and} \quad \frac{\mathrm{d}l'_{i,j}}{\mathrm{d}t^*} = G'^*(l'_{i,j}). \tag{27}$$

Therefore, the application of the EQMOM to the hyperbolic PBE in Eq. (14) is reduced to a set of ordinary differential equations written in terms of the weights $\varsigma'_{i,j}$ and abscissas $l'_{i,j}$. This approach has a major advantage in dealing with the shrinking-core model, Eq. (3), which depends on the outer particle size L. When a mono-sized approach is adopted, L is the same for all particles, hence no difficulty in the evaluation of G. However, when the modelling approach considers the PSD, L also has a distribution, which is the same as the initial PSD. Therefore, the evaluation of G requires a method to map a given (evolving) particle core size to the corresponding particle outer size, which corresponds to the initial value of the core size itself. In the present work, this mapping is done automatically when solving the initial-value problems in Eq. (27), because the value of L for the abscissas $l'_{i,j}$ is related to their (known) initial conditions. To explain further, one can think of a given abscissa $l'_{i,j}$ moving along its corresponding characteristic curve with a rate determined by the shrinking-core model, which depends on its corresponding value of L. Since $L = l|_{t=0}$, the value of L for abscissas is indeed related to their initial conditions, which in turn is computed from the initial particle size distribution. In this way, as mentioned previously, the polydispersity of particles is considered fully in the modelling framework, i.e., a varying distribution for l and a constant initial distribution for L.

Another important observation is that the weights $\varsigma'_{i,j}$ are constant over time, and therefore, $\hat{m}'_0$ is conserved as defined in Eq. (28). Thus, since $\hat{m}_0 = \hat{m}'_0$ following the definition of $\hat{f}'$ (i.e., $\hat{f}'\mathrm{d}l' = \hat{f}\mathrm{d}l$), it can be concluded that the conservation of $\hat{m}_0$ is automatically respected in this numerical solution approach. We remind the reader that some of the previous and following derivations depend on the fact that $\hat{m}_0$ is a conserved quantity.

It is noteworthy that the continuous representation of $\hat{f}'$, i.e., Eq. (20), can be reconstructed by first, calculating the moments of $\hat{f}'$ from the point representation,

$$\hat{m}'_k(l') = \sum_{i=1}^{N_\mathrm{q}} \sum_{j=1}^{N_i} \varsigma'_{i,j}(l'_{i,j})^k, \tag{28}$$

and then obtaining the parameters of the quadrature in Eq. (20), i.e., σ, w'_i and l'_i, by the EQMOM inversion algorithm described in the work of Nguyen et al. [22]. It is important to remind the reader that in this work, the EQMOM inversion algorithm is applied to the moments of $\hat{f}'$, which is a density function defined over the interval $[0,1]$. It should be mentioned that Eq. (28) is obtained by substituting Eq. (26) into Eq. (18), and therefore, N_i should be always larger than $N_\mathrm{q}+1$ to have the integration be exact for the moments up to order $2N_\mathrm{q}$. Combining this constraint on N_i with the previous one, we have $N_i \geq \max(N_\mathrm{q} + N_\mathrm{G}, N_\mathrm{q}+1)$.

Once a continuous $\hat{f}'(l')$ is reconstructed, the NDF can be obtained easily. First, the pseudo-PSD $\hat{f}(l)$ can be computed by using the definition of $\hat{f}'$, i.e., $\hat{f}'\mathrm{d}l' = \hat{f}\mathrm{d}l$, and Eq. (7). Then, the pseudo-NDF $\hat{n}(l)$ is calculated by $\hat{n} = \hat{m}_0\hat{f}$. Finally, the NDF $n(l)$ is simply the part of $\hat{n}(l)$ located in the positive size domain. In fact, as demonstrated in the next section, this procedure for the reconstruction of the NDF is indeed the main advantage of our proposed formulation of the EQMOM in terms of a transformed variable (l') that allows l to take negative values, which in turn is required for the idea of the pseudo-PSD shown in Fig. 2.

Moreover, the moments of the NDF (m_k) can be calculated by using the fact that n is the same as the pseudo-NDF $\hat{n}$ for $l \geq 0$, thus

$$m_k = \int_0^\infty l^k n(l)\mathrm{d}l = \hat{m}_0 \int_{\max(l_\mathrm{min},0)}^{l_\mathrm{max}} l^k \hat{f}(l)\mathrm{d}l. \tag{29}$$

The last integral can be expressed in terms of the non-dimensional distribution $\hat{f}'$ and transformed size l' as follows

$$m_k = \hat{m}_0 \int_{\max(0,-l_{\min}/\Delta l)}^{1} (l'\Delta l + l_{\min})^k \hat{f}'\mathrm{d}l' = \hat{m}_0 \bar{L}^k \int_{\max(0,-l^*_{\min}/\Delta l^*)}^{1} (l'\Delta l^* + l^*_{\min})^k \hat{f}'\mathrm{d}l', \tag{30}$$

with $\Delta l = l_{\max} - l_{\min}$ and $\Delta l^* = l^*_{\max} - l^*_{\min}$. By using the Gauss-Jacobi quadrature, we obtain

$$m_k = \hat{m}_0 \bar{L}^k \sum_{i=1}^{N_q} \sum_{j=1}^{N_i} \varsigma'_{i,j} (l'_{i,j}\Delta l^* + l^*_{\min})^k I_{[\max(0,-l^*_{\min}/\Delta l^*),1]}(l'_{i,j}), \tag{31}$$

where I is an indicator function that returns 1 for $l'_{i,j} \in [\max(0, -l^*_{\min}/\Delta l^*), 1]$ and 0 elsewhere, and therefore, only the positive part of the pseudo-NDF (which corresponds to the NDF) is used for the calculation of m_k. In other words, the integration in Eq. (31) is calculated by using those $l'_{i,j}$ that locate in the interval $[\max(0, -l^*_{\min}/\Delta l^*), 1]$, i.e., the interval that corresponds to the positive size. However, the more is the progress of the leaching reaction, the less is the number of abscissas in this interval. Therefore, N_i should be large enough to increase the accuracy of the integration in the entire duration of the process. This point should be considered over the criteria mentioned previously for N_i, because even if the integration over the full support (i.e., including also the ghost particles) can become exact with a certain number of quadrature points (for instance, as in the case of a polynomial G), the calculation of m_k might still lack enough accuracy. Nevertheless, the criteria introduced previously for N_i can be considered as sufficient in most cases, particularly when the absolute values of the moments are not needed. We will elaborate more about the choice of N_i in the Result and Discussion Section.

3.1. Coupling the EQMOM with the concentration balance

As mentioned in the previous section, the concentration of the leaching agent C_A in the solution is governed by Eq. (16), which is coupled with the PBE through the source term S^*. Here, we explain the calculation of S^* by starting from its definition reported in the previous section. Thus, we have

$$S^* = \frac{\tau S}{C^0_A} = \frac{\tau}{C^0_A}\frac{\rho_B}{b}\frac{\mathrm{d}V_c}{\mathrm{d}t} = k_v \tau \frac{\rho^*_B}{b}\frac{\mathrm{d}}{\mathrm{d}t}\int_0^\infty l^3 n \mathrm{d}l = k_v \tau \frac{\rho^*_B}{b}\frac{\mathrm{d}m_3}{\mathrm{d}t}, \tag{32}$$

with $\rho^*_B = \rho_B / C^0_A$. The last equality follows from the definition of the moments of the NDF in Eq. (17), which can be applied to the PBE in Eq. (1) to obtain

$$\frac{\mathrm{d}m_3}{\mathrm{d}t} + l^3 G(l) n(l)\Big|_0^\infty - \int_0^\infty 3l^2 G(l) n(l) \mathrm{d}l = 0. \tag{33}$$

The second term on the left-hand side of Eq. (33) is zero at both ends of the interval. Furthermore, by definition, the pseudo NDF $\hat{n}$ is the same as the NDF n for $l \geq 0$, thus

$$\frac{\mathrm{d}m_3}{\mathrm{d}t} = \int_0^\infty 3l^2 G(l) n(l) \mathrm{d}l = 3\hat{m}_0 \int_{\max(l_{\min},0)}^{l_{\max}} l^2 G(l) \hat{f}(l) \mathrm{d}l. \tag{34}$$

By making $\hat{f}$ and l dimensionless, we obtain

$$\frac{\mathrm{d}m_3}{\mathrm{d}t} = 3\hat{m}_0 \int_{\max(0,-l_{\min}/\Delta l)}^{1} (l'\Delta l + l_{\min})^2 G(l'\Delta l + l_{\min}) \hat{f}'\mathrm{d}l' = 3\frac{\hat{m}_0 \bar{L}^3}{\tau} \int_{\max(0,-l^*_{\min}/\Delta l^*)}^{1} (l'\Delta l^* + l^*_{\min})^2 G^*(l'\Delta l + l_{\min}) \hat{f}'\mathrm{d}l'. \tag{35}$$

The argument to G^* is intentionally left dimensional because G^* is related to G, which in turn depends on the dimensional size. Substituting Eq. (35) in Eq. (32) and using the Gauss-Jacobi quadrature, we obtain

$$S^* = 3k_v \hat{m}^*_0 \frac{\rho^*_B}{b} \sum_{i=1}^{N_q} \sum_{j=1}^{N_i} \varsigma'_{i,j} (l'_{i,j}\Delta l^* + l^*_{\min})^2 G^*(l'_{i,j}\Delta l + l_{\min}) I_{[\max(0,-l^*_{\min}/\Delta l^*),1]}(l'_{i,j}), \tag{36}$$

with $\hat{m}^*_0 = \hat{m}_0 \bar{L}^3$. The indicator function $I_{[\max(0,-l^*_{\min}/\Delta l^*),1]}$ guarantees that the ghost particles with negative core size do not contribute to the leaching reaction.

3.2. Calculation steps, implementation and computational demand

In summary, we integrate a system of dimensionless ordinary-differential equations comprised of Eqs. (10), (16) and (27) to obtain the change of $\varsigma'_{i,j}$, $l'_{i,j}$, $l^*_{\min}$, $l^*_{\max}$ and C^*_A over time. For this purpose, the calculation steps are as follows.

1. Given an initial NDF n^0 bounded to the interval $[l^0_{\min}, l^0_{\max}]$, compute $\hat{m}_0 = m_0|_{t=0}$ by using Eq. (17) and then calculate $\hat{f}'\Big|_{t=0} = \Delta l^0 \frac{n^0}{\hat{m}_0}$
2. Set the number of nodes N_q for the EQMOM quadrature
3. Compute the first $2N_q$ moments of $\hat{f}'$ by Eq. (18)
4. Apply the EQMOM inversion algorithm introduced by Nguyen et al. [22] to obtain $\sigma|_{t=0}$, $w'_i\Big|_{t=0}$ and $l'_i\Big|_{t=0}$
5. For each EQMOM quadrature node, compute $\alpha_i|_{t=0}$ and $\beta_i|_{t=0}$ and set the number of points for the Gaussian quadrature rule, i.e., N_i
6. Obtain the abscissas $x'_{i,j}\Big|_{t=0}$ and weights $w'_{i,j}\Big|_{t=0}$ of the Gauss-Jacobi quadrature for each EQMOM quadrature node by using $\alpha_i|_{t=0}$, $\beta_i|_{t=0}$ and N_i
7. Calculate $\varsigma'_{i,j}\Big|_{t=0}$ and $l'_{i,j}\Big|_{t=0}$ from $w'_i\Big|_{t=0}$, $w'_{i,j}\Big|_{t=0}$ and $x'_{i,j}\Big|_{t=0}$ as defined in Eq. (25)
8. Integrate Eqs. (10), (16) and (27) from $t = 0$ to $t = t_f$ with the initial conditions $\varsigma'_{i,j}\Big|_{t=0}$, $l'_{i,j}\Big|_{t=0}$, $l^*_{\min}\Big|_{t=0}$, $l^*_{\max}|_{t=0}$ and $C^*_A\Big|_{t=0}$

It should be mentioned that the derivatives of $l'_{i,j}$, $l^*_{\min}$ and $l^*_{\max}$ depend on $G(l,t)$, which in turn requires to know the corresponding outer size (L), for which a constant distribution should be taken into account. As mentioned previously, the distribution of the outer size (L) is the same as the distribution of the core size (l) at time zero. Therefore, for each $l'_{i,j}$, we have $L_{i,j} = l'_{i,j}\Big|_{t=0}(l^0_{\max} - l^0_{\min}) + l^0_{\min}$, see Eq. (7). Instead, for $l^*_{\min}$ and $l^*_{\max}$, the outer size L is equal to their initial conditions multiplied by $\bar{L}$, i.e., $L_{\min} = l^*_{\min}\Big|_{t=0}\bar{L} = l^0_{\min}$ and $L_{\max} = l^*_{\max}|_{t=0}\bar{L} = l^0_{\max}$.

Regarding the implementation, a Python code is developed to perform the above calculation steps. It includes a general class for the EQMOM with several functions aimed at inverting the set of moments to find the weights, abscissas and the parameter σ of the quadrature. Moreover, it has a method for returning the point representation of the NDF given a set of moments, and also a method for evaluating the reconstructed NDF. The EQMOM is implemented as a general class so that it can be instantiated for each test case studied in the following section. In fact, each test case is coded in a separate Python script that 1) pre-processes the initial NDF and sets the required parameters, e.g., those of the shrinking-core model; 2) instantiate an EQMOM class for the selected N_q and N_i; 3) integrates in time the dimensionless equa-

tions for the abscissas, concentrations, and bounds of the NDF by using the ordinary differential equation (ODE) solver of Scipy package, i.e., *solve_ivp*; 4) post-process the integration results and visualize them. The developed codes and the first studied test case are uploaded to a public repository [24].

Concerning the computational demand of the proposed approach, we restrict our attention to the solution of (tens to hundreds) ordinary differential equations as the most time-consuming calculation. The computational time of this calculation mainly depends on the stiffness of the problem (i.e., time-scale of the mechanisms in the shrinking-core model), process duration and ODE integration method. Among these factors, the stiffness of the problem has the largest effect. Thus, as long as the equations are not excessively stiff, the simulation time is not a matter of concern. Still one might be concerned about the computational time if one aims at coupling the proposed approach with the computational fluid dynamics (CFD), however, such a coupling is not feasible with the current formulation of the EQMOM adapted to the shrinking-core model. In fact, the description of the diffusion and convection of the fluid in a CFD simulation coupled with the EQMOM is done through the moments (not the weights and abscissa of the quadrature). As a result, the blending of the moments of cells in a CFD simulation by the diffusion and convection causes the loss of mapping between the distribution of the core size (l) and the distribution of the outer size (L), which is an essential aspect of the proposed approach to consider both distributions in evaluation of the shrinking-core model. Nevertheless, in this work, our focus is on spatially homogeneous stirred reactors, which is a valid assumption for the leaching process described by the shrinking-core model, because the time-scale of the mixing in a stirred reactor is presumably shorter than those of the mechanisms in the shrinking-core model.

3.3. Realizability issue

The realizability issue of moments is an important aspect of the QBMMs that deserves special discussion. Briefly, in the numerical solution of the PBE by moment-based methods, a set of predicted moments might assume certain values that cannot belong to any physical distribution, and therefore, inversion algorithms fail to find a quadrature approximation of the underlying NDF from that set of (non-realizable) moments. A more rigorous explanation employs the concept of the moment space, which is a convex space formed by all the possible moment sets (of a certain size denoted by N_{m}) of all the possible positive measures that can be defined on a particular support, e.g., $[0, 1]$ as in this work. Then, a given moment set is realizable if and only if it belongs to the moment space. Here, our aim is just to mention the concept of the moment space, which determines bounds on admissible values for moments, without discussing it in detail. A full discussion of the realizability issue and moment space is out of scope of this work, and can be found elsewhere [14,20,22,25–28].

While the realizability of moments is often a significant issue in spatially non-homogeneous simulations [18,25–28], it can also occur in spatially homogeneous systems, e.g., a leaching process in a well-stirred reactor. In the latter case, non-realizable moments might be predicted due to numerical errors such as those related to the numerical integration of equations. Moreover, the transport in the phase space can take the moment set close to the boundary of the moment space, which can create numerical difficulties.

Regarding the numerical integration, one can try to employ a more accurate integration method or tighten tolerances of the solver to decrease numerical errors as much as possible. In this work, the selection of integration tolerances, particularly the absolute ones, is an easy task since the variables are made non-dimensional with predictable order of magnitude. The only exception is l^*_{min} that can assume large negative values, however, its maximum order of magnitude can still be estimated a priori.

Concerning the realizability of moments, we should first remind the reader that in the approach proposed here, the EQMOM inversion algorithm is not needed during the integration of the governing equations in Eq. (10), Eq. (16) and Eq. (27), since Eq. (27) is written in terms of the quadrature parameters. In fact, the inversion of moments is done only once before starting the integration of the governing equations to obtain the initial value for the quadrature parameters, and then, the integration is performed until the final time without requiring to reuse the EQMOM inversion algorithm, i.e., the integration continues regardless of any potential realizability issue. Once the system of the ODEs is solved, the NDF at a selected time can be obtained by computing the moments $\hat{m}'_k(l')$ and then reconstructing $\hat{f}'$ from the moment set by using the EQMOM inversion algorithm, as explained earlier. This reconstruction fails if the computed moment set is non-realizable. In this case, the EQMOM inversion algorithm attempts to perform the reconstruction with a subset of the moment set that belongs to the moment space, i.e., disregarding high-order moments unless the moment set becomes realizable. This realizable subset of moments can be identified by examining the canonical moments since in this work, we deal with the Hausdorff moment problem, i.e., moment problem on the support $[0, 1]$. Briefly, in the Hausdorff moment problem, a set of moments belongs to the interior of the moment space if the associated canonical moments lie in the interval $(0, 1)$. The reader can find more information about canonical moments elsewhere [20,27,29]. Furthermore, as mentioned before, we employ the EQMOM inversion algorithm by Nguyen et al. [22] that was developed to deal with the boundary of the moment space. Therefore, it is expected that the adopted solution approach proves robust if a problematic moment set is predicted.

4. Results and discussion

In this section, we assess the proposed method by performing several numerical tests for which some analytical or reference solutions can be obtained. In addition, the method is used to simulate a leaching process for which some experimental data is available. Finally, we show that the method can be also applied to dissolution problems in which no inert layer forms around particles.

In all the following cases, the reaction is the one reported in Eq. (2). In addition, particles are assumed spherical, thus $k_v = \pi/6$. Moreover, the number of quadrature nodes (N_{q}) is set to more than three following the suggestion by Yuan and co-workers who found that the EQMOM with three or four nodes provides accurate predictions for the moments of the NDF for evaporation, in which the growth rate is negative as in leaching. The only exception is the third test case "Varying Concentration" with a uniform initial particle size distribution, where only two nodes are deliberately used in the EQMOM for the reason that is explained in the corresponding part. Regarding the ODE solver, a variant of Petzold's method [30] is used that switches automatically between (non-stiff) Adams and (stiff) backward differentiation formulas. This method is available in Scipy package by selecting the *LSODA* option of *solve_ivp* solver. Furthermore, the relative and absolute tolerances of the ODE solver and the initial time step is set to 10^{-6}, 10^{-8} and 0.001, respectively. These settings for the ODE solver lead to fast simulations of the following test cases, except the last one, i.e., dissolution controlled by liquid-film mass-transfer, that takes a bit longer due to the stiffness of the equations, as explained later.

4.1. Surface-reaction rate limited case

The first case is a leaching process controlled by the surface-reaction rate, in other words, negligible mass-transfer resistance in the inert layer and liquid film around particles. Under these conditions, Eq. (9) reduces to $G = -2bk_{\mathrm{s}}C_{\mathrm{A}}/\rho_{\mathrm{B}}$. Here, no decaying factor is considered for negative-size particles because all particles shrink with the same rate. Moreover, we assume that C_{A} is constant, i.e., A is present in excess.

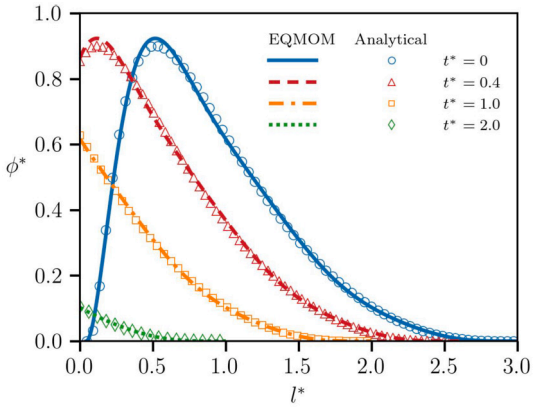

Fig. 3. The comparison of the dimensionless PSD predicted by the EQMOM against the analytical solutions at four selected times for shrinking-core particles in the surface-reaction controlling regime.

Therefore, G does not change over time. In this extreme case, the expected behaviour is that the PSD shifts with a constant rate to smaller values of particle size without changing its shape.

To perform the simulation, the initial NDF is assumed to have the form of a truncated log-normal distribution [15] as follows

$$n^0(l) = \frac{m_0|_{t=0}}{\ln \sigma_g^0 \sqrt{2\pi}} . \exp\left(- \frac{\left\{ \ln \left[\frac{(l - l^0_{\min})(l^0_{\max} - l^0_{\min})}{(l^0_{\max} - l)\bar{l}^0_g} \right] \right\}^2}{2(\ln \sigma_g^0)^2} \right), \tag{37}$$

where $l^0_{\min}$ and $l^0_{\max}$ are the bounds of the initial distribution. As $l^0_{\min} \to 0$ and $l^0_{\max} \to \infty$, Eq. (37) reduces to the log-normal distribution with $\bar{l}^0_g$ and σ^0_g being the geometric mean and geometric standard deviation, respectively [15]. In this first case, $l^0_{\min} = 0.45$ μm, $l^0_{\max} = 30$ μm, $\bar{l}^0_g = 10$ μm and $\sigma^0_g = 2.5$, which are very close to those reported by LeBlanc and Fogler [1] for the dissolution of Mn_2O_3. It should be mentioned that we use $\bar{l}^0_g$ as the length-scale, thus $\bar{L} = \bar{l}^0_g$.

LeBlanc and Fogler [1] showed that Eq. (4) can be solved analytically by the method of characteristics for the dissolution process (shrinking particles) in the surface-rate limiting regime, provided that the reacting solution contains a large excess amount of A. Since shrinking-core particles (as in the leaching process) behave the same as shrinking particles (as in the dissolution process) under the surface reaction controlling regime [16], we can use their approach to obtain the analytical solution for our case. The only difference is that here the variable is the size of particle core. By assuming that the initial PSD is a truncated log-normal distribution, LeBlanc and Fogler [1] derived an analytical solution for Eq. (4) in terms of the non-dimensional distribution $\phi^* = \bar{L} n / m_0|_{t=0}$, l^* and t^*. The advantage of these dimensionless variables is that the solution is independent of the individual values for $m_0|_{t=0}$, k_s, C^0_A, ρ_B and b as long as the concentration of A is excess enough to remain constant.

Fig. 3 compares the results obtained by the EQMOM versus the analytical solutions at four selected times. As expected, the non-dimensional PSD shifts to the left without changing the shape as the reaction proceeds. The EQMOM results are obtained by setting $N_q = 3$, which is large enough to match the quadrature approximation with the initial PSD satisfactorily, as depicted by the blue curve in Fig. 3. Moreover, since G is constant and independent of the core size, $N_i = 4$ for $i \in 1, 2, 3$ should suffice. In fact, Fig. 3 shows a very good agreement between the analytical solutions and EQMOM predictions at the selected times.

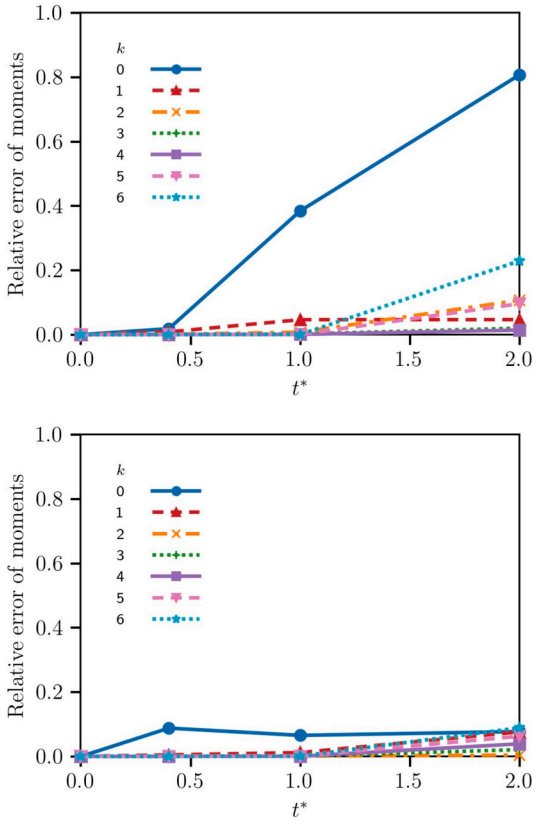

Fig. 4. The relative error of the first seven moments, i.e., $k \in 0, 1, \ldots, 6$ for $N_i = 4$ (top) and $N_i = 10$ (bottom), where N_i is the number of points of the Gaussian-Jacobi quadrature.

A supplementary insight can be obtained by comparing the predicted moments with the analytical ones. For this purpose we use the following expression

$$m_{k,\text{error}} = \frac{\left| m_{k,\text{predicted}} - m_{k,\text{analytical}} \right|}{m_{k,\text{analytical}}}. \tag{38}$$

The top graph in Fig. 4 shows the error defined by Eq. (38) for the first seven moments when $N_i = 4$. It is interesting that the error for all the moments increases as we advance in time, i.e., as more and more particles are leached. In fact, at $t^* = 4.0$, the error for some moments, in particular m_0, increases considerably. This might seem paradoxical because we observe a very good agreement between the predicted and analytical PSDs in Fig. 3, even at $t^* = 4.0$. In fact, as explained in the previous section, the NDF is obtained by taking the part of the pseudo-NDF located in the positive side of the size domain, and this pseudo-NDF is reconstructed by using all the abscissas $l'_{i,j}$ regardless of the time, which results in satisfactory predictions for the PSD, as shown in Fig. 3. However, as we advance in time, more and more abscissas exit the valid domain for the calculation of the moments of the NDF, see Eq. (31), and this has an adverse effect on the accuracy of the numerical integration in Eq. (31) to obtain moments. Indeed, by increasing the number of abscissas to ten, the accuracy of the predicted moments by Eq. (31) can be improved greatly, as shown by the bottom graph in Fig. 4 and also in Fig. S1(b) of the Supplementary Material. It should be mentioned that this argument is made to clarify better the effect of N_i on the moment values calculated by Eq. (31)) when they are sought, otherwise, $N_i = 4$ suffices to obtain a good accuracy for the predicted PSD in this test case.

4.2. Mixed controlling regimes

Here, we consider a problem similar to the previous case with the same initial NDF except that the mass-transfer resistance in the inert

layer is not negligible. In this case, we assume an identical timescale for both the surface reaction and mass-transfer through the inert layer, which yields $k_s/\mathscr{D}_e = 1.2 \times 10^6$ given that $\bar{L} = 10^{-5}$ m. Likewise, the concentration of A is assumed constant, i.e., A is supplied in excess amount. Moreover, no decaying factor is considered in Eq. (9), i.e., $c_d = 0$.

To our knowledge, no analytical solution exists for the evolution of the PSD in the case of mixed controlling regimes, and therefore, we can only discuss qualitatively the EQMOM predictions for the PSD. However, the conversion of B, X_B, can be calculated with the method used by Gbor and Jia [2], which we use as a reference solution for assessing the EQMOM predictions.

Here, we briefly explain the method to obtain the reference solution for X_B. At a given time t, the unreacted fraction of particles of outer size L, $g(L,t)$, is known by integrating Eq. (3) from time 0 to t. It is evident that $g(L,t)$ varies between 1 and 0. Moreover, the contribution of particles of outer size L to the cumulative conversion is proportional to their mass fraction, which in turn is known from the initial mass-based PSD. If C_A is constant and the leaching process is controlled by both the surface reaction and inert layer diffusion, then $g(L,t)$ can be obtained by [31]

$$\left[1-3[g(L,t)]^{2/3}+2g(L,t)\right]+\frac{12\mathscr{D}_e}{k_s L}\left[1-[g(L,t)]^{1/3}\right] = \frac{24b\mathscr{D}_e C_A}{\rho_B L^2}t, \quad \text{if } L > L_c(t) \tag{39}$$

with

$$L_c(t) = -\frac{6\mathscr{D}_e}{k_s}+\sqrt{\left(\frac{6\mathscr{D}_e}{k_s}\right)^2+\frac{24b\mathscr{D}_e C_A}{\rho_B}t}, \tag{40}$$

where, particles with outer size less than L_c are already leached completely, i.e., $g(L,t)=0$. Finally, X_B^{ref} can be expressed as

$$X_B^{ref}(t) = 1-\int_{\max(l^0_{min},L_c)}^{l^0_{max}} g(L,t)f_v^0(L)\mathrm{d}L, \tag{41}$$

where, $f_v^0(L)$ denotes the initial PSD (on a volume-size basis), which can be obtained from the initial NDF (which is on a number-size basis) as follows

$$f_v^0(L) = \frac{n^0(L)L^3}{\int_{l^0_{min}}^{l^0_{max}} n^0(L)L^3\mathrm{d}L}. \tag{42}$$

In the EQMOM, the conversion of B can be calculated by noting that

$$1-X_B(t) = \frac{\text{volume of unreacted cores at time } t}{\text{initial volume of particles}} = \frac{\int_0^\infty l^3 n(l;t)\mathrm{d}l}{\int_0^\infty l^3 n^0(l)\mathrm{d}l}. \tag{43}$$

The integrals in the denominator and numerator of Eq. (43) are the third moment of the NDF at time 0 and t, respectively. The former can be computed from the initial (known) NDF. The latter, instead, is calculated by using the EQMOM quadrature approximation for the NDF together with the Gauss-Jacobi quadrature rule, as previously detailed for the calculation of the source term of the concentration balance equation, which yields

$$\int_0^\infty l^3 n\mathrm{d}l = \dot{m}_0^* \sum_{i=1}^{N_q}\sum_{j=1}^{N_i} \varsigma'_{i,j}(l'_{i,j}\Delta l^* + l^*_{min})^3 I_{[\max(0,-l^*_{min}/\Delta l^*),1]}(l'_{i,j}). \tag{44}$$

Fig. 5 depicts the EQMOM predictions for $\phi^*(l^*)$ at four times. The EQMOM predictions are obtained by employing a five-node quadrature for the approximation of the NDF. In addition, we set $N_i = 10$ for the Gaussian quadrature rule, which is larger than the constraint introduced in the previous section since the shrinkage rate is not a polynomial. The first observation is that by increasing the number of nodes with respect to the previous test case (i.e., from three to five), the EQMOM approximation for the initial $\phi^*(l^*)$ matches perfectly the initial truncated log-normal distribution, though it is a marginal improvement with respect to the previous test case. As time passes, the distribution shifts to the left and additionally its peak shrinks down. This is an expected behaviour as reported elsewhere for the dissolution of particles under mixed controlling regimes [6].

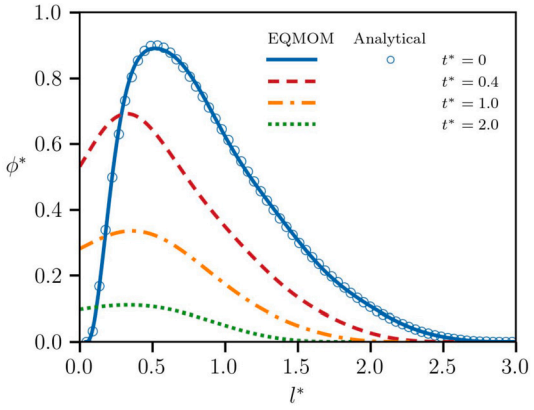

Fig. 5. Time evolution of the dimensionless PSD predicted by the EQMOM for shrinking-core particles with a shrinkage rate that depends on the surface-reaction and mass-transfer in the inert layer.

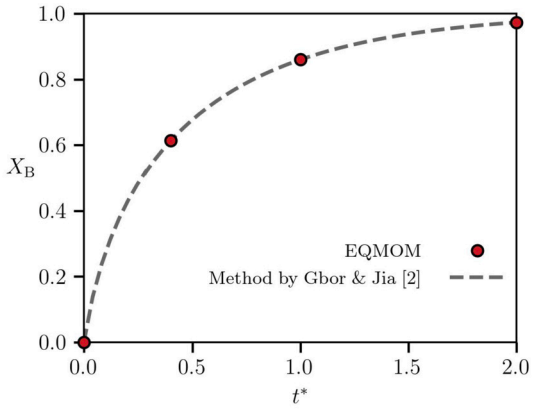

Fig. 6. The comparison of the leaching conversion predicted by the EQMOM against the reference solution obtained by the method proposed by Gbor and Jia [2]. The shrinkage rate of particle cores depends on the surface-reaction and mass-transfer in the inert layer.

As a quantitative evaluation, Fig. 6 shows a perfect agreement between the conversion of B predicted by the EQMOM at four selected times with the reference solution calculated by Eq. (41). This agreement supports the PSD predictions by the EQMOM in Fig. 5. Moreover, it shows that the integrals involving G can be calculated by using the Gaussian quadrature rule even when G is not a polynomial. Although in this case, a larger number of points have been used to achieve an acceptable accuracy.

4.3. Varying concentration

In the previous studied cases, we assumed that an excess amount of the leaching agent A existed in the solution, and therefore, its concentration did not change with time. This assumption was adopted to simplify the problems such that an analytical or a reference solution could be obtained for the sake of comparison. Now, we consider a case with a varying concentration of the leaching agent. In addition, we assume that the particles are distributed uniformly between l^0_{min} and

$l^0_{\max}$. Let us set these limits to 0 and 30 μm, respectively. In addition, the length-scale $\bar{L}$ is set to the average particle size, thus $\bar{L} = 15$ μm. Furthermore, we assume that the leaching process is controlled by the surface reaction, and therefore, G does not depend on the core and outer size of the particle although it changes over time due to variations in the concentration of A.

The choice of a uniform initial distribution and the assumption of surface-reaction controlling regime allow us to obtain a reference solution which in turn, can be used to provide a quantitative evaluation of the predictions. As mentioned earlier, in the case of the surface-reaction controlling regime, the initial NDF shifts to smaller sizes without changing the shape. Thus, assuming $l^0_{\min} = 0$, we have

$$n(l;t) = \begin{cases} \dfrac{m_0|_{t=0}}{l^0_{\max}}, & 0 < l \le l_{\max}(t) \\ 0, & l > l_{\max}(t) \end{cases}, \tag{45}$$

or in terms of non-dimensional variables,

$$\phi^*(l^*;t^*) = \begin{cases} \dfrac{1}{l^*_{\max}|_{t=0}}, & 0 < l^* \le l^*_{\max}(t^*) \\ 0, & l^* > l^*_{\max}(t^*) \end{cases}. \tag{46}$$

Therefore, the problem of computing ϕ^* reduces to finding $l^*_{\max}(t^*)$ by Eq. (10), which requires G^*, which in turn depends on C_A or equally its non-dimensional form, C^*_A. In addition, C^*_A is governed by Eq. (16), which depends on $\dfrac{dm_3}{dt}$. By using Eqs. (17) and (45), we obtain the following relation

$$\frac{dm_3}{dt} = \frac{d}{dt}\int_0^{\infty} l^3 n dl = \frac{m_0|_{t=0}}{l^0_{\max}}\frac{d}{dt}\int_0^{l_{\max}(t)} l^3 dl = \frac{m_0|_{t=0}}{l^0_{\max}}\frac{dl_{\max}(t)}{dt}[l_{\max}(t)]^3, \tag{47}$$

where, the last equality is derived by using the Leibniz integral rule [32].

Now by using Eqs. (10), (16), (32) and (47) and making variables non-dimensional, we can write the following system of ordinary differential equations for $l^*_{\max}$ and C^*_A

$$\begin{aligned} \frac{dl^*_{\max}}{dt^*} &= -C^*_A \\ \frac{dC^*_A}{dt^*} &= -k_v\frac{\rho^*_B}{b}C^*_A\frac{\hat{m}^*_0}{l^*_{\max}|_{t=0}}[l^*_{\max}(t)]^3, \end{aligned} \tag{48}$$

which can be solved by an initial-value problem solver to obtain a reference solution.

Fig. 7 depicts the time evolution of the non-dimensional PSD obtained by the EQMOM. In addition, Fig. 8 compares the values of C^*_A predicted by the EQMOM to its variation obtained by solving Eq. (48). As in the previous cases, the results are expressed in terms of the non-dimensional variables, ϕ^*, l^*, t^*, and C^*_A, therefore, they are independent of the selected value for k_s. However, they still depend on $m_0|_{t=0}$, ρ^*_B and b as indicated by Eq. (48). The results shown in Figs. 7 and 8 are obtained by setting them to 5×10^{13}, 5 and 1, respectively. Regarding the number of quadrature points, it is noteworthy that one beta kernel, Eq. (21) is enough to represent exactly a uniform distribution ($l'_1 = \sigma$ and $\sigma = 1/2$) [14]. Likewise, the size dependency of the summation of two beta kernels, Eq. (21), can vanish by setting $l'_1 = \sigma$, $l'_2 = 2\sigma$ and $\sigma = 1/3$. In fact, this can be extended to the summation of any number of beta kernels. Therefore, we can choose any positive integer for N_q. However, we intentionally adopt a two-node quadrature for this case, i.e., $N_q = 2$, for reasons to be given later. Accordingly, we set $N_i = 3$ for both quadrature nodes since G does not depend on the size.

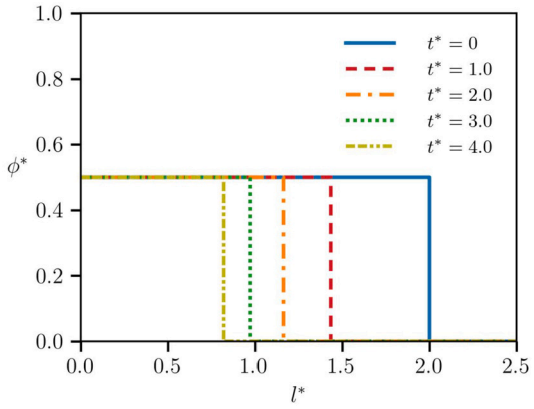

Fig. 7. Time evolution of the dimensionless PSD predicted by the EQMOM for shrinking-core particles in the surface-reaction controlling regime and under a varying concentration of the leaching agent.

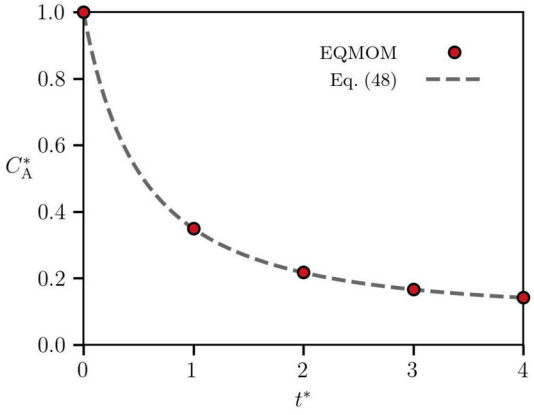

Fig. 8. The dimensionless concentration of the leaching agent predicted by the EQMOM against the reference solution obtained by Eq. (48) for shrinking-core particles in the surface-reaction controlling regime.

As expected, the initial uniform distribution shifts to the left with time. However, contrary to the first studied case, it shifts with a rate that slows down as the reaction proceeds, which is associated to the decrease in the concentration of A as shown in Fig. 8. Another observation is that the shape of the predicted PSDs in Fig. 7 remains uniform at later times, which demonstrates an improvement over the results presented in the original work by Yuan et al. [14] on the development of the EQMOM. In fact, they studied an evaporation problem with an initial uniform distribution and a constant shrinkage rate by using a four-node quadrature, i.e., $N_q = 4$, as they intended to evaluate the error when $N_q > 1$. In that case, the EQMOM did not predict the exact uniform distribution, and instead four peaks (attributed to each quadrature node) appeared in the predicted size distribution. However, they showed that the problem could be alleviated by increasing the number of points of the Gauss-Jacobi quadrature, although the rippling pattern still persisted to exist. In contrast, in the present work, the uniform shape is maintained through the course of the simulation despite the fact that $N_q > 1$. This superior reconstruction of the NDF is indeed attributed to the use of the pseudo-NDF, see Fig. 2, which requires to consider ghost particles (i.e., particles with negative core size) in the calculations, which in turn is achieved by formulating the EQMOM in terms of the transformed variable l', as detailed in the previous section.

In addition, the comparison between the EQMOM predictions and the reference solution for C^*_A shows a perfect agreement, which verifies the calculations, and in particular the integrals, done in the EQMOM.

Concerning the accuracy of the predictions for the individual moments, we can likewise make the same argument about N_i as that we

presented previously in the first studied test case. In fact, it is expected that $N_i = 3$ is not sufficient to obtain accurate results for the individual moments by Eq. (31) in spite of the perfect predictions for the PSD. In line with this expectation, Fig. S3(a) of the Supplementary Material shows that the accuracy of the predictions for m_0 diminishes in time. However, Fig. S3(b) of the Supplementary Material shows that the accuracy of the predicted m_0 is improved considerably by increasing N_i to ten, as it results in a more accurate numerical integration in Eq. (31), as explained earlier. Again, we emphasize that here our aim of increasing N_i is to show its effect on the predicted moments obtained by Eq. (31) if their individual values are needed. Otherwise, as shown in Figs. 7 and 8, $N_i = 3$ is enough to obtain a good accuracy for the predicted PSD and solution concentration.

4.4. Leaching example

After previous numerical analyses, we use the EQMOM to simulate a real leaching experiment conducted by Yoon et al. [33]. They studied the leaching of neodymium (Nd) from the oxidized E-scrap of NdFeB magnets in H_2SO_4 solutions according to the following reaction [33]

$$3\,H_2SO_4 + Nd_2O_3 \longrightarrow Nd_2(SO_4)_3 + 3\,H_2O. \tag{49}$$

In the conducted experiments, they measured the conversion of Nd (denoted by X_B) versus time at some selected H_2SO_4 concentrations and temperatures. Moreover, they used excess amounts of H_2SO_4, and therefore, C_A is assumed to be constant.

According to their observations, the shrinking-core model can be used to describe the process because the initial particle size distribution differs only slightly from that measured after the completion of the leaching. By assuming that the diffusion in the inert layer controls the leaching process, they used the following relation in terms of X_B to obtain an apparent rate constant for the diffusion, k_d (1/min) at the investigated conditions

$$1 - 3(1 - X_B)^{2/3} + 2(1 - X_B) = k_d t, \quad \text{and} \quad k_d = \frac{8\mathscr{D}_e C_A}{\rho_B L^2} \tag{50}$$

It should be highlighted that the above relation is valid for mono-sized particles and a constant concentration of C_A. Finally, they estimated an apparent activation energy by plotting k_d versus temperature for selected concentrations of A, which was found to be relatively low. In this way, they justified their assumption about the controlling step of the process.

Contrary to the mono-sized approach adopted by Yoon et al. [33], we take into account the polydispersity of particles with the help of the EQMOM. Indeed, this allows to highlight the importance of considering the PSD in the modelling of the leaching process. For this purpose, we use the measured conversion data for one of the experimental conditions investigated by Yoon et al. [33], $C_A = 3$ M and $T = 30\,^{\circ}$C. In addition, we extract the particle size distribution plotted in figure 6 of their work. It is noteworthy that they reported the volume percent versus particle size, and therefore, the extracted data is converted to a number-based density distribution before being used in the EQMOM. In addition, based on the experimental PSD, l^0_{min} and l^0_{max} are set to 0.26 and 100 μm, respectively.

Since no information is provided for $\mathscr{D}_e$ and ρ_B by Yoon et al. [33], the shrinking-core model is modified as follows

$$G(l,t) = \begin{cases} \dfrac{-\bar{L}}{\left[\tau_r + \dfrac{6\tau_d}{\bar{L}}(l - l^2/L)\right]}, & l > 0 \\ \dfrac{-\bar{L}}{\tau_r}\exp(c_d l^*), & l \le 0 \end{cases} \tag{51}$$

where, $\tau_r = \dfrac{\rho_B \bar{L}}{2bC_A k_s}$ and $\tau_d = \dfrac{\rho_B \bar{L}^2}{24bC_A\mathscr{D}_e}$ with $b = 1/3$. Comparing the definition of τ_d with that of k_d in Eq. (50) yields $\tau_d = k_d^{-1}$. Although the diffusion in the inert layer is the controlling step, we include a negligible surface-reaction resistance ($\tau_r \ll \tau_d$) to avoid numerical issues at small sizes ($l \to 0$). Here, we set $\tau_r/\tau_d = 10^{-4}$ that is small enough to have no effect on the results. Moreover, since the surface-reaction resistance is negligible, c_d is adjusted to 10 in order to control the width of the pseudo-PSD as explained in the previous section. We have found that $c_d = 10$ is a good choice to avoid an excessive decrease of l_{min}. Lastly, $\bar{L}$ is set to 9.4 μm, which is the mean diameter of particles reported by Yoon et al. [33].

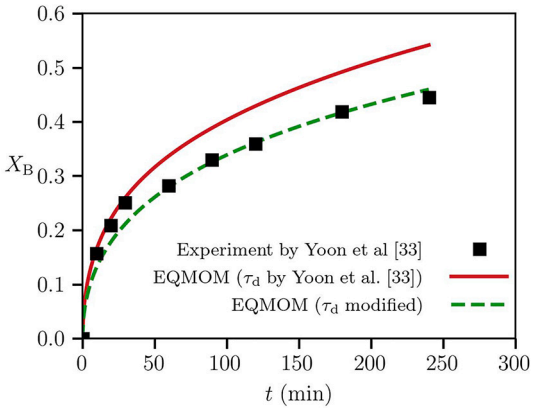

Fig. 9. The conversion of the leaching process predicted by the EQMOM (solid red and dashed green curves) against the experimental values (black squares) reported by Yoon et al. [33]. The agreement between the EQMOM predictions and the experimental data can be improved by modifying the mass-transfer time-scale obtained by Yoon et al. [33] via a mono-sized modelling approach.

For the quadrature approximation of the PSD, we use 4 nodes, i.e., $N_q = 4$. And for the Gauss-Jacobi quadrature, we employ $N_1 = 100$ and $N_2 = N_3 = N_4 = 10$. The reason behind choosing a large number of Gaussian quadrature points for the first node, i.e., $N_1 = 100$, is to obtain a smooth profile for the predicted moments, particularly the moment of order zero (see Fig. S4 of the Supplementary Material). It is noteworthy that Yuan et al. [14] also employed large number of Gaussian quadrature points for the first and second nodes to improve the accuracy of predictions in the case of evaporation, i.e., size shrinkage.

Fig. 9 compares the predicted conversion of Nd obtained by using two different values of τ_d against the measured data. The red curve in Fig. 9 is predicted by using $\tau_d = 2987$ min, which corresponds to $k_d = 3.348 \times 10^{-4}$ as reported by Yoon et al. for the selected experimental condition [33]. The discrepancy between this curve and the measurements can be attributed to the employed τ_d, and therefore, it is modified to examine potential improvements in the results. For this experimental condition, a satisfactory agreement between the predictions and the experiments is found by using $\tau_d = 5078$ min, which is 70% larger than the value reported by Yoon et al. [33]. This fact highlights the significance of considering the PSD in the modelling of the leaching process, and the importance of methods that allow us to do this.

4.5. Dissolution controlled by liquid-film mass-transfer

In the last studied case, we use the EQMOM method to simulate the dissolution process, i.e., shrinking particles. In this case, no inert layer is considered around particles, and therefore, the core size l corresponds to the particle outer size L. Assuming the Stokes regime, the shrinkage of the particle size can be described by

$$G(l,t) = \begin{cases} \dfrac{-2bC_A}{\rho_B\left[\dfrac{1}{k_s} + \dfrac{l}{2\mathscr{D}}\right]}, & l > 0 \\ \dfrac{-2bC_A k_s}{\rho_B}\exp(c_d l^*), & l \le 0 \end{cases} \tag{52}$$

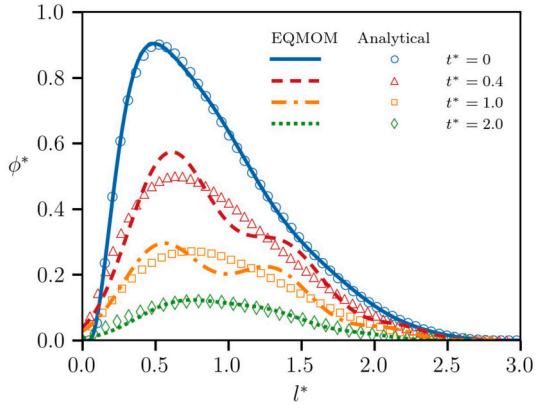

Fig. 10. The comparison of the dimensionless PSD predicted by the EQMOM against the analytical solutions at four selected times for shrinking particles (dissolution process) in the mass-transfer controlling regime.

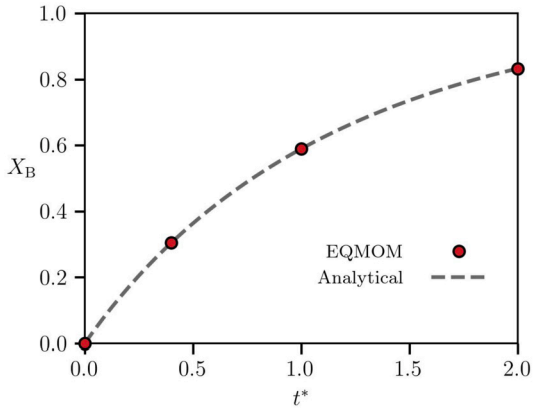

Fig. 11. The comparison of the conversion predicted by the EQMOM against the analytical solution for shrinking particles (dissolution process) in the mass-transfer controlling regime.

where $\mathscr{D}$ is the diffusion coefficient of A in the liquid film around particles. It is noteworthy that Eq. (52) can be obtained from the shrinking-core model, Eq. (9), by assuming no inert layer resistance, $l \equiv L$ and $k_f = \frac{2\mathscr{D}}{l}$. The last expression is the Stokes law regime.

In the following, we consider that the mass-transfer in the liquid-film is the controlling step, i.e., $k_f \ll k_s$. The reason is that if the process is controlled by the surface-reaction, the behaviour of both shrinking and shrinking-core particles is identical [16], and therefore, the results shown previously for shrinking-core particles in the surface-reaction controlling regime apply equally to shrinking particles. In addition, the concentration of A is assumed constant, so that an analytical solution can be obtained for the sake of comparison.

The initial NDF is the truncated log-normal distribution shown in Eq. (37). This choice allows to use the analytical solution obtained by LeBlanc and Fogler [1] for the dissolution of particles. The parameters of the truncated distribution are the same as those reported in the first studied case (see section 4.1). Likewise, the results are expressed in terms of the non-dimensional variables ϕ^*, l^* and t^*, and therefore, they do not depend on the individual values for $m_0|_{t=0}$, $\mathscr{D}$, C_A^0, ρ_B and b as long as the concentration of A is excess enough to remain constant. To avoid numerical issues at small particle sizes, a negligible surface-reaction resistance equivalent to a relatively large k_s is employed in Eq. (52), i.e., $k_s = 10^3 \frac{2\mathscr{D}}{\bar{L}}$. We have observed that the results change negligibly by decreasing further the surface-reaction resistance (i.e., increasing k_s), however the stiffness of equations increases too much, which in turn makes the ODE solver too slow. Moreover, due to a negligible surface-reaction resistance, c_d is set to 10 to avoid the excessive decrease in the (negative) size of ghost particles, in other words, to avoid the excessive increase of the width of the pseudo-NDF.

Fig. 10 compares the results obtained by the EQMOM versus the analytical solutions at four selected times. The EQMOM results are obtained by setting $N_q = 4$. Moreover, N_i was set to 80 for the first two quadrature nodes ($i = 1, 2$) and 40 for the last two ($i = 3, 4$). We use such number of points for the Gaussian quadrature rule to increase the accuracy of integrations since G is not polynomial in this case. As can be seen from Fig. 10, a very good agreement is obtained between the predicted and analytical solutions for ϕ^* at all the selected times. At $t^* = 0.4$ and 1.0, the predicted distribution becomes multimodal, hence causing some deviation between the predicted PSD and the analytical one – that appear as some ripples around the analytical solution. It is clearly associated to the approximation of the underlying PSD by a quadrature, i.e., a summation of some density functions. In fact, the shape of the quadrature is manifested strongly in those predictions. Nevertheless, Fig. 11 confirms that these deviations have negligible effect on the average properties of the particle population, as the predicted values for the conversion match perfectly the analytical values at the selected times. Both the analytical and predicted values are obtained by using Eq. (43). Moreover, the predicted values of the moments are very close to the analytical ones as the moment error defined in Eq. (38) is below 0.044 for all the moments at all the selected times. For instance, Fig. S5 of the Supplementary Material shows a very good agreement between the predicted and analytical solutions for m_0.

The results confirm that the proposed method performs well in simulating the dissolution process under both surface-reaction and mass-transfer limiting regimes, and therefore, we expect similar performance in general cases in which both mechanisms play a role in the dissolution of particles. It is noteworthy that the particle breakage can also be described by the EQMOM in the case of shrinking particles, following the procedure detailed by Yuan et al. [14], which is an advantage over the other approaches mentioned in the introduction section.

5. Conclusions

We have presented a modified version of the extended quadrature method of moments (EQMOM) to solve the population balance equation (PBE) for the description of shrinking-core particles in the leaching process. In fact, we have shown that the EQMOM can naturally address the dependency of the shrinking-core model on the particle core size (with an evolving distribution) and outer size (with a constant distribution), and therefore, it allows us to use this model in the PBE without any mathematical complexity.

The main advantage of the proposed approach is that it requires no specific assumption on the limiting step or the operating conditions, as demonstrated by the different test cases studied in this work. Another advantage is the superior performance with respect to the original EQMOM developed by Yuan et al. [14] as exhibited in the case of a leaching process with an initial uniform particle size distribution (PSD). This superior performance is attributed to the fact that the proposed approach considers also particles with a negative core size, which has been implemented through the definition of the pseudo-NDF, the transformation of the internal coordinate (i.e., size) and the modification of the shrinking-core model.

In summary, the obtained predictions for the PSD and conversion in the studied test cases prove this approach promising for solving a PBE that describes shrinking-core particles in the leaching process. In addition, it has been shown that the same approach can be employed to solve the PBE for the dissolution process, i.e., shrinking particles.

In an upcoming study, we plan to employ this approach to simulate a leaching process of a Hydrometallurgical recycling route for lithium-ion batteries. Furthermore, the proposed approach can be extended to applications described by the shrinking core-shrinking particle model [34] that requires to solve a bi-variate PBE written in terms of both the core size and outer size of particles.

CRediT authorship contribution statement

Mohsen Shiea: Writing – review & editing, Writing – original draft, Visualization, Validation, Software, Methodology, Formal analysis, Conceptualization. **Luigi Crema:** Writing – review & editing, Supervision, Project administration, Funding acquisition. **Edoardo Gino Macchi:** Writing – review & editing, Writing – original draft, Supervision, Resources, Project administration, Funding acquisition.

Declaration of competing interest

The authors declare that they have no known competing financial interests or personal relationships that could have appeared to influence the work reported in this paper.

Data availability

I have shared the link to a public repository of the developed codes in the submitted manuscript.

Acknowledgements

The result presented in this paper is part of FREE4LIB project (Feasible REcovery of critical raw materials through a new circular Ecosystem FOR a Li-Ion Battery cross-value chain in Europe). This project has received funding from Horizon Europe research and innovation programme under Grant Agreement No. 101069890. Views and opinions expressed are those of the authors only and do not necessarily reflect those of the European Union or CINEA. Neither the European Union nor the granting authority can be held responsible for them.

Appendix A. Supplementary material

Supplementary material related to this article can be found online at https://doi.org/10.1016/j.ces.2024.119987.

References

[1] S. LeBlanc, H.S. Fogler, Population balance modeling of the dissolution of polydisperse solids: rate limiting regimes, AIChE J. 33 (1) (1987) 54–63.
[2] P.K. Gbor, C.Q. Jia, Critical evaluation of coupling particle size distribution with the shrinking core model, Chem. Eng. Sci. 59 (10) (2004) 1979–1987.
[3] J.E. Sepulveda, J.A. Herbst, A population balance approach to the modeling of multistage continuous leaching systems, in: AIChE Symp. Ser., vol. 74, 1978, pp. 41–65.
[4] F. Crundwell, Progress in the mathematical modelling of leaching reactors, Hydrometallurgy 39 (1–3) (1995) 321–335.
[5] D.H. Rubisov, V.G. Papangelakis, Mathematical modelling of the transient behaviour of cstrs with reactive particulates: part 1—the population balance framework, Can. J. Chem. Eng. 74 (3) (1996) 353–362.
[6] M. Giona, A. Adrover, F. Pagnanelli, L. Toro, A closed-form solution of population-balance models for the dissolution of polydisperse mixtures, Chem. Eng. J. 87 (3) (2002) 275–284.
[7] M. Hänchen, S. Krevor, M. Mazzotti, K.S. Lackner, Validation of a population balance model for olivine dissolution, Chem. Eng. Sci. 62 (22) (2007) 6412–6422.
[8] F. Crundwell, A. Bryson, The modelling of particulate leaching reactors—the population balance approach, Hydrometallurgy 29 (1–3) (1992) 275–295.
[9] F.E.B. Coelho, J.C. Balarini, E.M.R. Araújo, T.L.S. Miranda, A.E.C. Peres, A.H. Martins, A. Salum, Roasted zinc concentrate leaching: population balance modeling and validation, Hydrometallurgy 175 (2018) 208–217.
[10] D. Ramkrishna, Population Balances: Theory and Applications to Particulate Systems in Engineering, Elsevier, 2000.
[11] W. Zhao, M.A. Jama, A. Buffo, V. Alopaeus, Population balance model and experimental validation for reactive dissolution of particle agglomerates, Comput. Chem. Eng. 108 (2018) 240–249.
[12] A.L. Dale, G.V. Lowry, E.A. Casman, Accurate and fast numerical algorithms for tracking particle size distributions during nanoparticle aggregation and dissolution, Environ. Sci. Nano 4 (1) (2017) 89–104.
[13] D.L. Marchisio, R.D. Vigil, R.O. Fox, Quadrature method of moments for aggregation–breakage processes, J. Colloid Interface Sci. 258 (2) (2003) 322–334.
[14] C. Yuan, F. Laurent, R. Fox, An extended quadrature method of moments for population balance equations, J. Aerosol Sci. 51 (2012) 1–23.
[15] A. Randolph, M.A. Larson, Theory of Particulate Processes: Analysis and Techniques of Continuous Crystallization, 2nd edition, Academic Press, an Imprint of Elsevier, San Diego, 1988.
[16] O. Levenspiel, Chemical Reaction Engineering, 3rd edition, John Wiley & Sons, 1999.
[17] R.O. Fox, F. Laurent, M. Massot, Numerical simulation of spray coalescence in an Eulerian framework: direct quadrature method of moments and multi-fluid method, J. Comput. Phys. 227 (6) (2008) 3058–3088.
[18] M. Shiea, A. Querio, A. Buffo, G. Boccardo, D. Marchisio, CFD-PBE modelling of continuous Ni-Mn-Co hydroxide co-precipitation for Li-ion batteries, Chem. Eng. Res. Des. 177 (2022) 461–472.
[19] D.L. Marchisio, R.O. Fox, Computational Models for Polydisperse Particulate and Multiphase Systems, Cambridge University Press, 2013.
[20] M. Pigou, J. Morchain, P. Fede, M.-I. Penet, G. Laronze, New developments of the extended quadrature method of moments to solve population balance equations, J. Comput. Phys. 365 (2018) 243–268.
[21] E. Madadi-Kandjani, A. Passalacqua, An extended quadrature-based moment method with log-normal kernel density functions, Chem. Eng. Sci. 131 (2015) 323–339.
[22] T.T. Nguyen, F. Laurent, R.O. Fox, M. Massot, Solution of population balance equations in applications with fine particles: mathematical modeling and numerical schemes, J. Comput. Phys. 325 (2016) 129–156.
[23] W.H. Press, S.A. Teukolsky, W.T. Vetterling, B.P. Flannery, Numerical Recipes: The Art of Scientific Computing, 3rd edition, Cambridge University Press, 2007.
[24] M. Shiea, E. Macchi, The extended quadrature method of moments for the simulation of the leaching process, https://github.com/mshiea/leaching_eqmom, 2023.
[25] D.L. Wright Jr, Numerical advection of moments of the particle size distribution in Eulerian models, J. Aerosol Sci. 38 (3) (2007) 352–369.
[26] O. Desjardins, R.O. Fox, P. Villedieu, A quadrature-based moment method for dilute fluid-particle flows, J. Comput. Phys. 227 (4) (2008) 2514–2539.
[27] D. Kah, F. Laurent, M. Massot, S. Jay, A high order moment method simulating evaporation and advection of a polydisperse liquid spray, J. Comput. Phys. 231 (2) (2012) 394–422.
[28] M. Shiea, A. Buffo, M. Vanni, D.L. Marchisio, A novel finite-volume tvd scheme to overcome non-realizability problem in quadrature-based moment methods, J. Comput. Phys. 409 (2020) 109337.
[29] H. Dette, W.J. Studden, The Theory of Canonical Moments with Applications in Statistics, Probability, and Analysis, John Wiley & Sons, New York, 1997.
[30] L. Petzold, Automatic selection of methods for solving stiff and nonstiff systems of ordinary differential equations, SIAM J. Sci. Stat. Comput. 4 (1) (1983) 136–148.
[31] P.K. Gbor, Behaviour of Co, Ni, Cu and Fe during aqueous SO_2 leaching of non-ferrous smelter slag, Ph.D. thesis, University of Toronto, 2003.
[32] M. Abramowitz, I.A. Stegun (Eds.), Handbook of Mathematical Functions with Formulas, Graphs, and Mathematical Tables, Dover Publications, New York, 1972.
[33] H.-S. Yoon, C.-J. Kim, K.W. Chung, S.-J. Lee, A.-R. Joe, Y.-H. Shin, S.-I. Lee, S.-J. Yoo, J.-G. Kim, Leaching kinetics of neodymium in sulfuric acid from e-scrap of NdFeB permanent magnet, Korean J. Chem. Eng. 31 (2014) 706–711.
[34] V. Safari, G. Arzpeyma, F. Rashchi, N. Mostoufi, A shrinking particle—shrinking core model for leaching of a zinc ore containing silica, Int. J. Miner. Process. 93 (1) (2009) 79–83.